Capillary rise of a viscoplastic fluid in a Hele-Shaw cell

N. J. Balmforth[a]

[a] *Department of Mathematics, University of British Columbia, Vancouver, BC, V6T 1Z2, Canada*

Abstract

The capillary-driven rise between two plates of a yield-stress fluid modelled by the Herschel-Bulkley constitutive law is considered. For the geometry of a relatively narrow (Hele-Shaw) cell, the mathematical problem simplifies considerably, the dynamics being captured by a viscoplastic generalization of Darcy's law. This formulation can be used to determine the height of rise within a cell with varying gap thickness. In the limit that the gap varies over a wider scale than the height to which the fluid can rise, the problem reduces to one-dimensional, viscoplastic capillary rise, the solution of which has been given previously and compared with experiments. More generally, the dynamics is richer, with the capillary pressures causing fluid to first rise and then plug up parts of the cell.

1. Introduction

Capillary imbibition is conveniently illustrated by allowing a wetting fluid to be drawn into the gap between two closely spaced, vertical plates. For a viscous fluid, imbibition ceases when the capillary pressure driving ascent becomes hydrostatically balanced. The final height of rise is then controlled by the thickness of the gap, because that dimension sets the shape of the meniscus, and therefore the driving capillary pressure. The expression relating the height of rise to the gap thickness is often referred to as Jurin's law. If the cell is not uniform, the final height becomes set by the local gap, and varies with position. In these "Hele-Shaw" cells, the governing equations of viscous fluid mechanics also simplify considerably, setting the scene for complementary theoretical modelling.

When the fluid has, in addition, a yield stress, the driving capillary stress must overcome both gravity and the implied rheological barrier during imbibition [1, 2]. The final height of viscoplastic capillary rise therefore depends not only on the local gap, but also the yield stress. Whilst interrogating experiments with Carbopol suspensions in wedge-shaped slots, Géraud *et al.* [2], sought to disentangle the effects of the local gap and yield stress by formulating a relatively simple, viscoplastic generalization of Jurin's law. Although viscoplastic versions of the Hele-Shaw approximation for viscous fluid mechanics have been provided previously [3, 4, 5], and can be applied to this problem, Géraud *et al.* proceed more qualitatively by treating each vertical section of the slot independently. Though relevant to the construction of the final height of rise for a viscous fluid, this procedure implicitly ignores horizontal variations along the slot, which potentially limits its applicability.

The goal of the present work is to explore viscoplastic capillary imbibition along a Hele-Shaw cell with varying gap, using the viscoplastic version of the conventional Hele-Shaw reduction [3, 4, 5]. In doing so, gradients along the slot are consistently incorporated. The final height of rise is found by considering when the flux through the slot becomes arbitrarily small, which corresponds to an approach to the perfectly plastic limit of the model when there is a yield stress. As found for the spreading of viscoplastic fluids with a free surface over an inclined plane [6, 7], the limiting plastic problem recovers a version of the eikonal equation, which can be solved analytically using Charpit's method [8]. This strategy leads to a consistent generalization of Jurin's law for a narrow slot in which the usual assumptions of the Hele-Shaw reduction remain valid. Nevertheless, some pitfalls are encountered along the way which reveal a richer dynamics to viscoplastic capillary imbibition.

2. Mathematical formulation

Consider a two-dimensional, incompressible, Herschel-Bulkley fluid flowing between two plates with variable separation. A Cartesian coordinate system is aligned with the midsection, so that the $z-$axis points vertically upwards and the $y-$axis is the horizontal coordinate along the slot, (the $x-$axis is perpendicular to the midsection). Gravity acts in the $z-$direction, but fluid is pulled upwards against this body force by capillary effects.

When the cell has a characteristic thickness H that is much less than the characteristic lengthscale L along the slot, an asymptotic expansion can be performed to furnish a reduced model for the flow dynamics (*e.g.* [5]): in dimensionless form, the fluid pressure, denoted by $p(y, z, t)$, is nearly uniform across the gap and the flux, $\mathbf{q} = (q_{\rm y}, q_{\rm z})$, satisfies the slot-averaged conservation of mass equation,

$$\frac{\partial q_{\rm y}}{\partial y} + \frac{\partial q_{\rm z}}{\partial z} = 0. \tag{1}$$

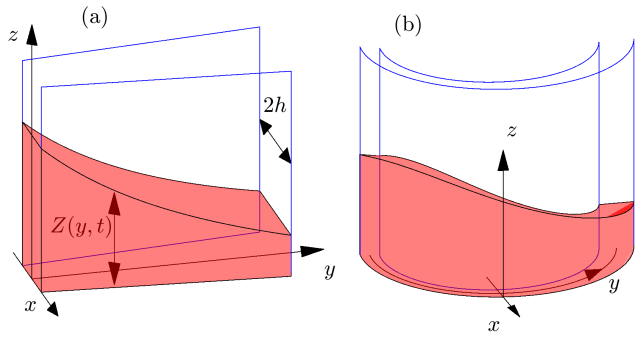

Figure 1: Sketch of the geometry describing the gap for (a) a tapered slot, and (b) offset cylinders.

The flux and pressure gradient $\boldsymbol{\nabla} p$ are related by

$$\mathbf{q} = -\frac{Q}{S}\begin{pmatrix} p_y \\ p_z + 1 \end{pmatrix}, \tag{2}$$

where $Q = |\mathbf{q}|$, $S = \sqrt{p_y^2 + (1+p_z)^2}$, and

$$Q(S; \mathrm{Bi}, n) = \frac{(n+1)hS + n\mathrm{Bi}}{(n+1)S^2}[\mathrm{Max}(hS - \mathrm{Bi}, 0)]^{1+\frac{1}{n}}. \tag{3}$$

Here, $2h$ denotes the local gap width and we have used subscripts as shorthand for partial derivatives, except for the flux, where the Roman style for the font highlights the significance as component. This dimensionless form is furnished by scaling y and z with a lengthscale L, x and h by H, pressure p by $3\mu_* UL/H^2$, and the deviatoric stress components by $3\mu_* U/H$, where U is a characteristic speed scale along the slot and

$$\mu_* = \tfrac{1}{3}K\left(2 + \tfrac{1}{n}\right)^n \left(\frac{U}{H}\right)^{n-1} \tag{4}$$

is a measure of the effective viscosity, expressed in terms of the consistency K and power-law index n of the Herschel-Bulkley model. The velocity scale is chosen so that

$$U = \frac{\rho g H^2}{3\mu_*}, \tag{5}$$

and the lengthscale L characterizes the height to which the fluid would rise in the absence of the yield stress,

$$L = \frac{\gamma \cos\Theta}{\rho g H}, \tag{6}$$

where γ is the surface tension and Θ is the contact angle. The dimensionless yield stress, or Bingham number, is

$$\mathrm{Bi} = \frac{\tau_Y H}{3\mu_* U}, \tag{7}$$

where the original yield stress is τ_Y.

The flux-gradient relation in (3) is illustrated in figure 2. The switch that arises for $S = \mathrm{Bi}h^{-1}$ corresponds to the yield point; if $S < \mathrm{Bi}h^{-1}$, the fluid is unyielded and a rigid plug bridges across the local gap to block any flow. For $\mathrm{Bi} = 0$, we obtain the flux-gradient relation for a power-law fluid, and if, in addition, $n = 1$, we recover the Newtonian law $Q = h^3 S$.

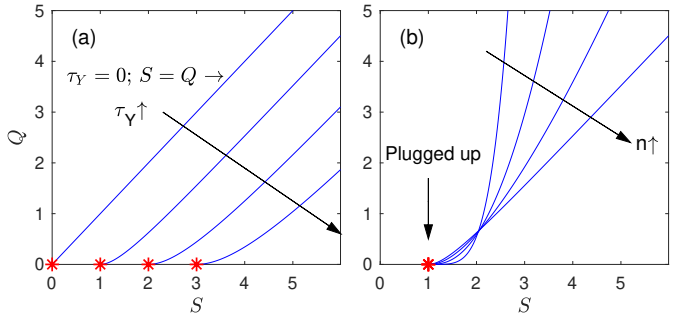

Figure 2: Flux functions for different (a) Bingham numbers $\mathrm{Bi} = 0$, 1, 2 and 3 (with $n = 1$) and (b) different power-law exponents $n = \frac{1}{4}$, $\frac{1}{2}$, $\frac{3}{4}$ and 1 (with $\mathrm{Bi} = 1$).

The fluid extends from a bath at $z = 0$ up the slot to a free surface at elevation $z = Z(y,t)$. In view of the preceding scalings, and ignoring atmospheric pressure, the boundary conditions at the underlying bath and the overlying interface are

$$p(y,0,t) = 0, \qquad p(y,Z,t) = -\frac{1}{h}, \tag{8}$$

$$Z_t + q_y(y,Z,t)Z_y = q_z(y,Z,t). \tag{9}$$

The second condition in (9) assumes that, locally to the free surface, the meniscus is pulled into a cylindrical shape dictated by the contact angle.

We consider the specific situation that the gap width, $2h(y)$, is independent of height, as illustrated in figure 1. The two sketches in this figure illustrate two configurations of particular interest: a wedge-shaped slot and the eccentric annular gap between two offset cylinders.

3. Uniform slots

Neglecting any horizontal variations in y, we find that $q_z = Q(t)$, and so $S = S(t)$. Therefore, $p = -z[1 + S(t)]$. The top surface conditions then indicate that

$$Z_t = Q(S; \mathrm{Bi}, n) \qquad \& \qquad hZ(1+S) = 1. \tag{10}$$

Consequently,

$$Z_t = Q[(hZ)^{-1} - 1; \mathrm{Bi}, n]. \tag{11}$$

The form of the flux function indicates that Z must increase upto the height where $Z_t \to 0$, or $S = \mathrm{Bi}/h$. The equilibrium height is

$$Z = \frac{1}{h + \mathrm{Bi}}, \qquad \text{or} \qquad \tilde{Z} = \frac{\gamma\cos\Theta}{\rho g \tilde{h} + \tau_Y} \tag{12}$$

in dimensional form (denoted with the tilde decoration). This last result is given by Geraud *et al.* [2].

Looking at the progress to the final state (with $hS \to \mathrm{Bi}$ and $Z < (h+\mathrm{Bi})^{-1}$),

$$Q \sim \frac{(2n+1)h^2}{(n+1)\mathrm{Bi}}(hS-\mathrm{Bi})^{1+\frac{1}{n}}, \tag{13}$$

and so

$$Z_t \sim \frac{h^2(2n+1)}{\mathrm{Bi}(n+1)}(h+\mathrm{Bi})^{1+\frac{1}{n}}(1-hZ-\mathrm{Bi}Z)^{1+\frac{1}{n}}, \tag{14}$$

implying the algebraic dependence,

$$Z \sim \frac{1}{h+\mathrm{Bi}} - (h+\mathrm{Bi})^{-2n-2}\left[\frac{n(n+1)h^2\mathrm{Bi}}{(2n+1)t}\right]^n. \tag{15}$$

By comparison, in the Newtonian problem, with $Q = h^3S$,

$$Z_t\left(\frac{hZ}{1-hZ}\right) = h^3, \tag{16}$$

or

$$\log(1-hZ) + hZ = -h^4 t, \tag{17}$$

indicating $Z \sim h^{-1} - Ce^{-h^4 t}$ for $t \gg 1$. The switch from exponential decay in (17) to algebraic decay in (15) highlights how the capillary rise is much slowed by the yield stress. Note that (17) implies that $ZZ_t \sim h^2$ for $Z \ll 1$, which increases with h, but the final height of rise is higher for smaller h. This suggests that, in a cell with variable gap, a Newtonian film will rise first in the widest part of the gap before slowing and being overtaken by the flow through the narrowest side. This uneven rise results because, as the gap narrows, the viscous resistance increases more strongly than the driving capillary pressure. The feature also carries over to the viscoplastic version of the problem and is evident in the numerical solutions of initial-value problems reported later.

Another noteworthy point is that final Newtonian state given by (17) ($Z = h^{-1}$, $Q = S = 0$ and $p = -z$), also applies when the gap is not uniform. This feature arises because (1) is solved exactly by this solution even if $h = h(y)$. Thus, to construct the final rise of height for a viscous fluid, once can consider each vertical cross-section of the slot independently. By contrast, the nonlinearity of the constitutive law for a viscoplastic fluid, which leads to the more complicated flux-pressure-gradient relation in (3), prevents any such construction when there is a yield stress. Instead, one must consider the states arising when the flux becomes arbitrarily small, which corresponds to the perfectly plastic limit of the model, as discussed next.

4. Limiting plastic states

Flow in the slot ceases ($Q \to 0$) when $Sh = \mathrm{Bi}$. Thus,

$$\frac{\mathrm{Bi}^2}{h^2} - \Upsilon^2 - (1+\Xi)^2 = 0, \quad \Upsilon = p_y, \quad \Xi = p_z, \tag{18}$$

which is a nonlinear first-order partial differential equation similar to the eikonal equation that can be solved by Charpit's method [8]: the characteristic equations are

$$\frac{\mathrm{d}y}{\mathrm{d}\zeta} = -2\Upsilon, \quad \frac{\mathrm{d}z}{\mathrm{d}\zeta} = -2(1+\Xi), \tag{19}$$

$$\frac{\mathrm{d}p}{\mathrm{d}\zeta} = -2\Upsilon^2 - 2\Xi(1+\Xi), \tag{20}$$

$$\frac{\mathrm{d}\Upsilon}{\mathrm{d}\zeta} = \frac{2\mathrm{Bi}^2 h'}{h^3}, \quad \frac{\mathrm{d}\Xi}{\mathrm{d}\zeta} = 0, \tag{21}$$

where ζ denotes a coordinate lying along each characteristic curve and $h' \equiv \mathrm{d}h/\mathrm{d}y$. From these relations, we find

$$z = z_0 - 2(1+\Xi)\zeta, \tag{22}$$

$$\Xi = \Xi_0, \tag{23}$$

$$\Upsilon = \varsigma\mathrm{Bi}\sqrt{h^{-2} - h_*^{-2}}, \tag{24}$$

where $\zeta = 0$ and $(y, z, p, \Upsilon, \Xi) = (y_0, z_0, p_0, \Upsilon_0, \Xi_0)$ refers to a point on the characteristics where some boundary information is available, and

$$h_* = -\frac{\mathrm{Bi}}{\Xi_0 + 1} \qquad \text{and} \qquad \varsigma = \mathrm{sgn}(h'). \tag{25}$$

Then,

$$\frac{\mathrm{d}z}{\mathrm{d}y} = \frac{1+\Xi}{\Upsilon} = -\frac{\varsigma h}{\sqrt{h_*^2 - h^2}}, \quad \frac{\mathrm{d}p}{\mathrm{d}y} = \Upsilon + \Xi\frac{\mathrm{d}z}{\mathrm{d}y}, \tag{26}$$

which can be reduced to quadrature.

In particular, provided the characteristic curve intersects the base of the slot, $z = 0$, where the fluid is in contact with the underlying bath, then we may take $z_0 = p_0 = \Upsilon_0 = 0$, in which case $h_* = h(y_0)$ and we arrive at

$$\begin{aligned} z &= \varsigma\int_y^{y_0} \frac{h\mathrm{d}y}{\sqrt{h_*^2 - h^2}} \\ p &= -z - \varsigma h_*\mathrm{Bi}\int_y^{y_0} \frac{\mathrm{d}y}{h\sqrt{h_*^2 - h^2}}. \end{aligned} \tag{27}$$

The capillary pressure condition at $z = Z(y)$ now demands that

$$\begin{aligned} Z &= \varsigma\int_y^{y_0} \frac{h\mathrm{d}y}{\sqrt{h_*^2 - h^2}} \\ \frac{1}{h} &= Z + \varsigma h_*\mathrm{Bi}\int_y^{y_0} \frac{\mathrm{d}y}{h\sqrt{h_*^2 - h^2}}, \end{aligned} \tag{28}$$

which dictates $Z(y)$ once the parameter y_0 is eliminated.

Note that if $h' = 0$ at $(y, z) = (y_0, 0)$, then (19) and (21) imply that $\Upsilon = 0$, $h = h_* = h(y_0)$ and $y = y_0$ for all ζ. That is, at any extremum in the gap thickness, the characteristic curve becomes a vertical straight line. Equation (20) now gives $p = -z(1 + \mathrm{Bi}/h_*)$ and $Z = (h_* + \mathrm{Bi})^{-1}$, as for a uniform slot. This result also follows from (27) and (28), though more circuitously.

4.1. Wedges

For a tapered slot (figure 1(a)), we set $h = \mathcal{L}^{-1}(y+\alpha)$, where $\mathcal{L}$ is the dimensionless horizontal length of the cell; *i.e.* H is chosen to be the net change in width, with the minimum dimensional width $2Hh(0) = 2\alpha H/\mathcal{L}$ set by the dimensionless parameter α. In this case, $\varsigma = 1$ and the integrals in (27)-(28) may be evaluated analytically to find that the characteristic curves are the circles,

$$(y_0+\alpha)^2 = z^2 + (y+\alpha)^2, \tag{29}$$

and the pressure is

$$p = -z - \tfrac{1}{2}\mathrm{Bi}\mathcal{L}\ln\left[\frac{\sqrt{z^2+(y+\alpha)^2}+z}{\sqrt{z^2+(y+\alpha)^2}-z}\right]. \tag{30}$$

The free surface is given by the implicit equation

$$\frac{\mathcal{L}}{y+\alpha} = Z + \tfrac{1}{2}\mathrm{Bi}\mathcal{L}\ln\left[\frac{\sqrt{Z^2+(y+\alpha)^2}+Z}{\sqrt{Z^2+(y+\alpha)^2}-Z}\right]. \tag{31}$$

For $(y+\alpha)^2 \gg Z^2$, this reduces to (12), corresponding to the limit that the slot is relatively long in comparison to the capillary climb. When $(y+\alpha)^2 \ll Z^2$, on the other hand, we find $Z \sim h^{-1}$, which corresponds to the Newtonian limit. Evidently, when the interface elevation becomes too steep, lateral pressure gradients can no longer be ignored, forcing a departure from the quasi-uniform-slot solution in (12). In particular, as illustrated in figure 3 for the case $\alpha = 0$, this approximation becomes dangerous as $y \to 0$ and the gap closes.

Nevertheless, there are two issues hidden within the solution (29)-(31): first, the characteristic curves emanating from the bath at $z = z_0 = 0$ no longer reach the free surface, but instead intersect the minimum gap at $y = 0$ for some $y_0+\alpha < y_c(\mathcal{L},\mathrm{Bi})$, as illustrated in figure 3(a). Above the final characteristic with $y_0+\alpha = y_c(\mathcal{L},\mathrm{Bi})$ (shown as the dashed line in the plot), the free surface no longer lies along characteristics beginning at the bath, but is instead intersected by curves connected to $y = 0$. Problematically, this indicates that it is no longer consistent to pin the characteristics at $z = 0$ and use the boundary information $z_0 = p_0 = \Upsilon_0 = 0$, as has been used to arrive at (29)-(31). Second, the characteristic beginning at $y = \mathcal{L}$ curves upward and leftward to smaller y, leaving a region to its right without any solution. Filling this region with the characteristics from (29)-(31) demands these curves begin along the open side of the slot at $y = \mathcal{L}$, and again possess inconsistent starting conditions. The two problematic regions are shown shaded in figure 3(a).

One possible resolution of both issues is to generate a second family of characteristics by beginning at $y_0 = 0$ or $\mathcal{L}$, with parameter $z = z_0$, and setting $p_0 = 0$ and $\Xi_0 = 0$ there. These conditions mimic a termination of the slot at the sides at atmospheric conditions. However, such starting conditions imply that the associated pressure field is independent of height ($p_z \equiv \Xi = \Xi_0 = 0$), in conflict with the solution elsewhere. A more involved analysis of the side edges at $y = 0$ and $y = \mathcal{L}$ therefore seems needed. Rather than proceed down this route, we instead abandon the wedge-shaped slot and consider a different problem in which the side conditions are more transparent.

4.2. Off-set cylinders

For a slot composed of two cylinders with almost equal radii, but offset axes (figure 1(b)), the gap is given by

$$h(y) = 1 - a\cos\theta, \quad y = \frac{\mathcal{L}\theta}{2\pi}, \quad -\pi \le \theta < \pi, \tag{32}$$

after choosing H as the average half-thickness of the gap and assuming that the cylinders' radii are relatively large in comparison (permitting the neglect of the cylinders' curvature). The dimensionless parameter a controls the offset of the cylinders, or equivalently the variation of gap. In this case, we avoid the need for any conditions at the side of the slot, demanding periodic boundary conditions in y instead.

With $\mathcal{L} = 1$ and $a = 4\pi^{-2}$, the characteristic curves constructed from (28) are shown in figure 4. As remarked earlier, because $h'(\pm\frac{1}{2}\mathcal{L}) = h'(0) = 0$, the characteristic curves leaving the widest and narrowest positions along the gap ($\theta = \pm\pi$ and $\theta = 0$) are vertical. In widest sections, the curves curves spread out from $y = \pm\frac{1}{2}\mathcal{L}$. Over the narrowest section ($\theta = 0$), however, the curves converge to $y = 0$ and are given approximately by

$$y \approx y_0 \cos\left[\frac{2\pi z}{\mathcal{L}\sqrt{a^{-1}-1}}\right], \tag{33}$$

for $y_0 \ll 1$. The characteristics therefore cross at $y = 0$ for

$$z \ge \tfrac{1}{4}\mathcal{L}\sqrt{a^{-1}-1} \tag{34}$$

(see figure 4).

Provided Bi is sufficiently large that the free surface lies below the crossing point implied by (34) (which demands that $\mathrm{Bi} > a-1+4/(\mathcal{L}\sqrt{a^{-1}-1})$, given that $Z(0) = (1-a+\mathrm{Bi})^{-1}$ here), the Charpit construction provides a complete pressure solution for the limiting state. The solution with $\mathrm{Bi} = 3$ in figure 4 shows one such example. Lowering Bi however, to the second solution with $\mathrm{Bi} = 2$ leads to a free surface that still intersects the characteristics field along curves that begin at the bath, but also includes a section along the minimum gap where the characteristics have crossed. This conflict is problematic for the pressure field as it implies that the associated solution is multi-valued unless the characteristics are terminated where they meet at $y = 0$. But rendering the solution single-valued in this manner still leaves a "scar" in the pressure field, with associated jumps in the horizontal pressure gradient (as illustrated by the corners evident in the isobars at $y = 0$ plotted for $\mathrm{Bi} = 2$), the consequences of which are unclear.

At still lower Bi (*e.g.* $\mathrm{Bi} = 1.5$ and 1 in figure 4), pieces of the free surface no longer intersect characteristics starting at the bath, reintroducing the complication observed

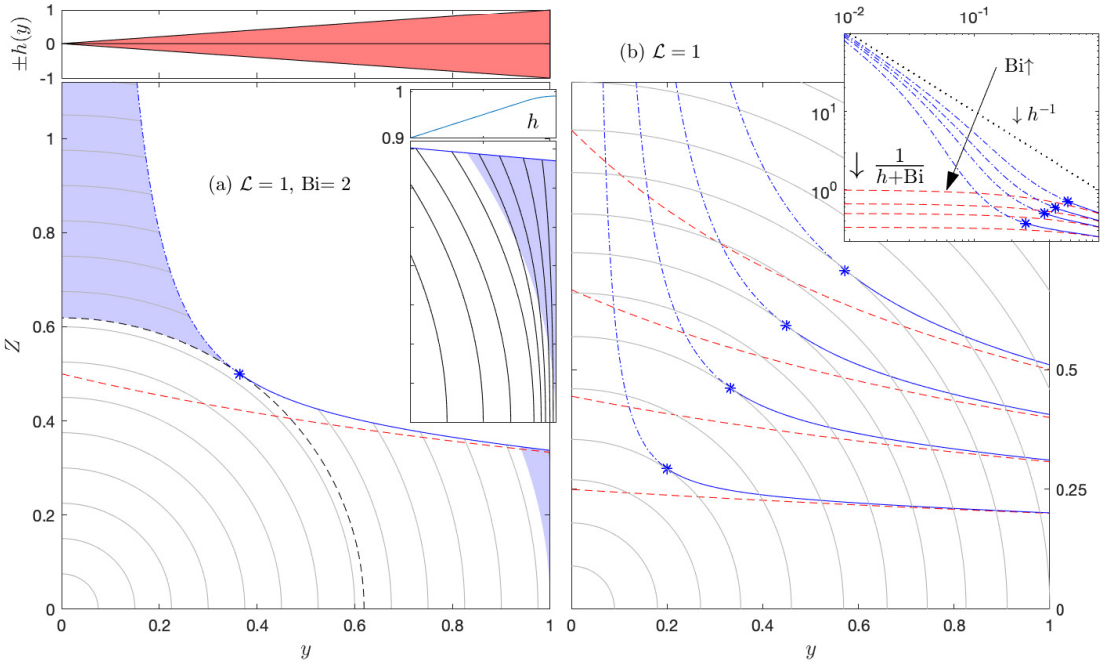

Figure 3: Capillary rise solutions (blue, solid) to (31) for $\mathcal{L}=1$ and $\alpha=0$ (leading to the gap shown at the top left), with (a) Bi = 2, and (b) varying Bingham number (Bi = 0.5, 1, 2 and 5). The red dashed lines show the uniform-slot result (12). In (a), the light grey lines show the characteristics in (29). The black dashed line is the last curve from the bath ($z=0$) that intersects the free surface (at the position marked by a star). Above this circle, the characteristics no longer reach the base but emerge from the side of the slot where $h\to 0$; here, the solution from (29) is drawn as a dot-dashed lines. The last characteristic from the side of the bath at $(y,z)=(\mathcal{L},0)$ also isolates a region against the right edge where information must arrive from that side. The regions where the characteristics do not start along the bath are shaded in light blue. The inset in (a) shows how a fan appears near $y=1$ when the gap is rounded off as indicated. The inset in (b) replots the data logarithmically and the dotted line shows the Newtonian limit $Z\sim h^{-1}$.

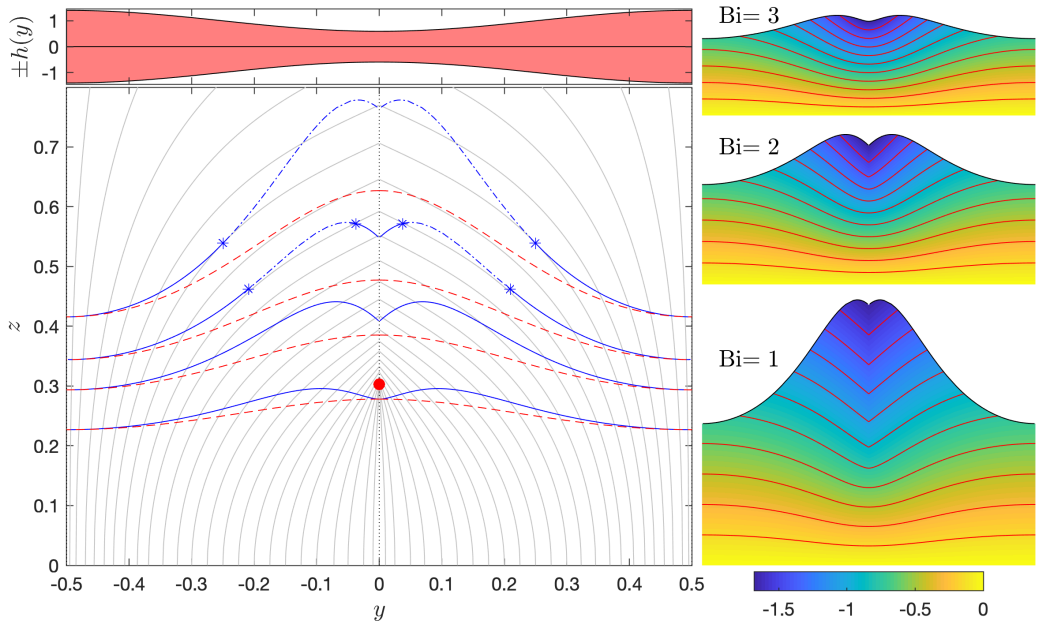

Figure 4: Capillary rise solutions (blue, solid) to (28) for an eccentric annular slot with $a=4\pi^{-2}$ and $\mathcal{L}=1$ (leading to the gap shown at the top left) for Bi = 1, 1.5, 2 and 3. The light grey lines show the characteristics from (28); red dashed lines show the uniform-slot result (12). The sections of the free surface for Bi = 1 and 1.5 lying along characteristics that do not start along the bath are plotted as dash-dotted lines. The red circle indicates the first elevation for which the characteristics cross at $y=0$. The panels to the right show density plots and isobars of the pressure field predicted by the Charpit solution, for the values of Bi indicated.

at high elevations for the wedge-shaped slot. Now, however, we cannot appeal to any side boundary conditions to build an alternative family of characteristics, the line $y = 0$ simply corresponding to the minium gap. Moreover, above the last characteristic that first meets the free surface tangentially (with intersection points marked by stars in figure 4), the Charpit construction fails: no information is available to complete the solution and locate the free surface. In figure 4, the pieces of the free surface shown by dot-dashed lines are inconsistent and cannot be trusted as they are constructed by continuing the characteristics from the bath through parts of the slot that are empty of fluid. Instead, the free surface here must be dictated by how the fluid was emplaced during the capillary rise, forcing us to solve the initial-value problem discussed in the next section.

Note that the spreading out of the characteristics from $y = \pm\frac{1}{2}\mathcal{L}$ ensures that the solution can always be constructed around the the widest part of the slot. The same construction applies to different slot shapes, with the rounding off of h' at the widest positions always leading to a set of diverging characteristics filling the gap there. As the scale over which h' is rounded becomes smaller, this set of characteristics limits to an expansion fan emerging from the small window of corresponding values of y_0. Thus, the problem noted earlier for a wedge-shaped slot regarding the shaded region on the right in figure 3(a) can be resolved by adding an expansion fan there, as illustrated by the inset to that panel.

5. Numerical results

5.1. Numerical scheme and application to the rise of a viscous fluid

To resolve the issues raised by the discussion of the limiting plastic states, it is convenient to turn to numerical solutions of (1), (3), (8) and (9), treated as an initial-value problem. More specifically, consider the periodic gap given by (32) with $a = 4\pi^{-2}$ and $\mathcal{L} = 1$, Bingham fluid with $n = 1$, and the initial condition, $Z(y, 0) = 0.05$.

The computational problem is broken down into two parts. First, at each moment in time, and given the instantaneous interface position $z = Z(y, t)$, equation (1) can be solved as a spatial boundary-value problem, subject to the two conditions in (8). To ease this task, the vertical coordinate z is first mapped onto a fixed rectangular domain by defining $\xi = z/Z(y, t)$. A fixed grid is then introduced in y, and the fast Fourier transform exploited to evaluate spatial derivatives in that direction. This turns (1) into a set of coupled ODEs in ξ, that can be solved using MATLAB's in-built solver bvp5c. The grid in y has 128 points; bvp5c introduces an adaptive grid with a variable number of points for ξ. The switches in the flux-pressure-gradient relation (3) are also smoothed by replacing $Q(S; \mathrm{Bi}, 1)$ in (1) by $\sqrt{Q^2 + \varepsilon^2}$, where ε is a small regularization parameter. Practically, ε is chosen to be 10^{-4} or smaller, and the effect of this regularization is gauged by varying the precise value. If no plugs appear, the regularization parameter can be set to zero in the computation without repercussions. When plugs do appear, the solutions are insensitive to the regularization, except as indicated later. The regularization also leads to a prescribed pressure solution over the plug, which would otherwise be indeterminate.

In the second part of the computation, the solution for the pressure is used to construct the flux at the interface. The third relation in (9) is then employed to advance the interface postion $z = Z(y, t)$ in time, using a simple, first-order, semi-Lagrangian scheme. A variable, but constrained, time step Δt is used based on the instantaneous maximum speed of the surface: $\Delta t = \mathrm{Min}(10^{-3}, 0.01/\mathrm{Max}(Q)))$.

We first present a solution for the Newtonian problem. Figure 5 shows a numerical solution for viscous fluid ($\mathrm{Bi} = 0$). Plotted are time series of the interface position at the minimum and maximum gaps, together with a set of snapshots of the full interface and the pressure distribution. At early times, the pressure field develops a fully two-dimensional structure. Simultaneously, the fluid rises first over the narrow sides of the gap, before the rise at the widest gap takes over at later times, as anticipated in §3. However, the two-dimensionality of the pressure field ensures that the evolution is not quantitatively predicted by (17) (see panel (a)). Eventually, the interface approaches the steady state given by $Z = h^{-1}$, with the pressure becoming independent of y, as again anticipated in §3.

5.2. Capillary rise with a yield stress

Computations for the viscoplastic case are shown in figures 6, 7 and 8. The first of these figures considers the case $\mathrm{Bi} = 3$, which, according to the analysis in §4 should develop into a doubly peaked, limiting plastic state without any crossed characteristics. Indeed, as shown in figure 6, the fluid rises under the capillary pressure, with the interface developping two peaks to either side of the minimum gap, once the flow through the narrow side of the gap overtakes that at the higher side. Eventually, the stresses everywhere decline to the yield point (given by $S = h\mathrm{Bi}$; *cf.* the final panel), and the interface approaches the steady state predicted by the Charpit analysis. Because the characteristics correspond to lines along which $\Xi_\zeta = 0$, those curves can be traced out for the numerical solution by plotting contours of constant vertical pressure gradient $\Xi = p_z$, as also indicated in figure 6.

In the second example of figure 7, the limiting plastic state is predicted to contain characteristics that cross over a higher section through the minimum gap (see figure 4). The Charpit analysis relieves the implied conflict by inserting a discontinuity into the pressure gradient there. For the numerical solution of the initial-value problem, evolution proceeds initially in a similar to that for higher Bi, with two peaks again forming to either side of the minimum gap. At later times ($t > 1.24$), however, the stresses fall below the yield point near the bottom of this section

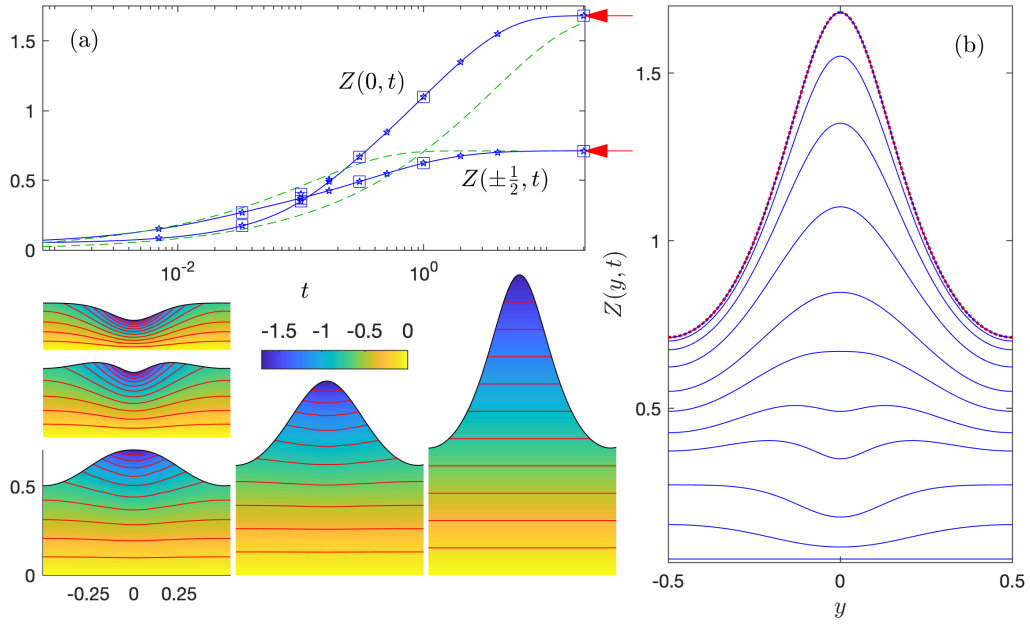

Figure 5: Capillary rise solutions for Newtonian fluid ($n = 1$, $\mathrm{Bi} = 0$) in the gap given by (32) with $a = 4\pi^{-2}$ and $\mathcal{L} = 1$, showing (a) times series of $Z(0,t)$ and $Z(\pm\frac{1}{2},t)$, and (b) snapshots of $Z(y,t)$ at the times indicated by stars in (a). The (red) dotted lines and arrows indicate the final steady state, $Z = h^{-1}$; the lighter (green) dashed lines in (a) show the result in (17). The lower left panel shows five snaphsots the pressure field (equally spaced isobars in red) at the times indicates by the squares in (a).

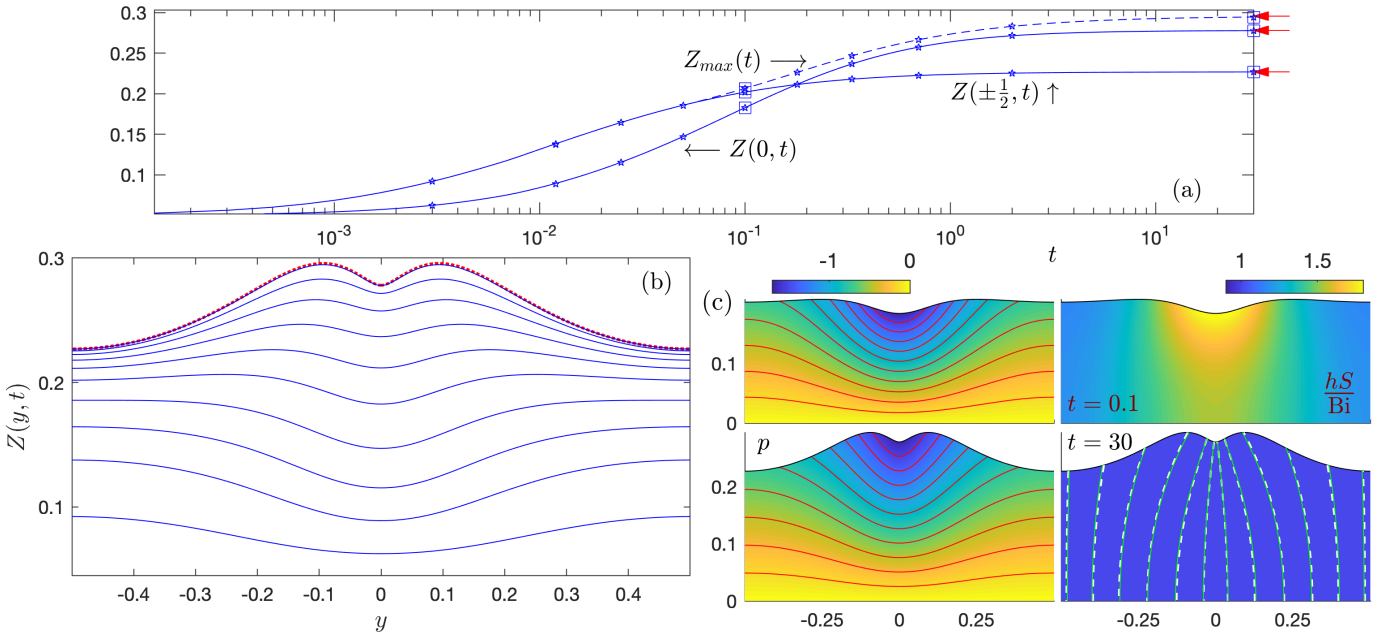

Figure 6: Capillary rise solutions for Bingham fluid ($n = 1$) with $\mathrm{Bi} = 3$, $a = 4\pi^{-2}$ and $\mathcal{L} = 1$ ($\varepsilon = 0$). Shown are (a) times series of $Z(0,t)$, $Z(\pm\frac{1}{2},t)$ and $Z_{max}(t) = \mathrm{Max}_y(Z)$ and (b) snapshots of $Z(y,t)$ at the times indicated by stars in (a). The (red) dotted lines and arrows show the limiting plastic solution of §4. Panel (c) shows two snaphsots of p and hS/Bi (isobars in red) at the times indicated (squares in (a)). In the final snapshot of hs/Bi, the light green lines show some of the characteristics from figure 4, and the white dashed lines show correspondingly chosen contours of constant p_z.

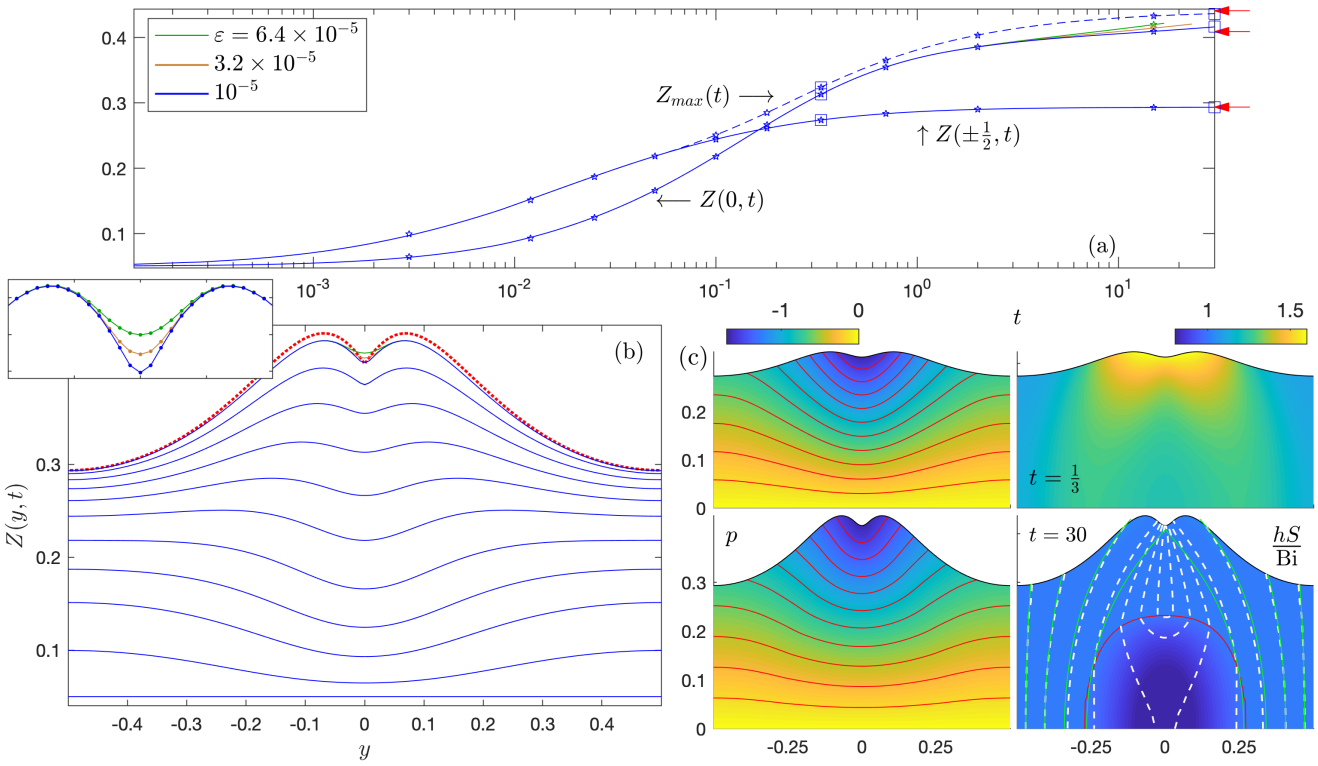

Figure 7: A similar figure to that shown in figure 6, but for Bi = 2. In this case, three solutions are shown with different values of the regularization parameter ε (as indicated); these are indistinguishable, except near $y = 0$ at the latest times. The inset to (b) shows a magnification of the final computed interfaces around the minimum gap, with the grid points indicated by dots. Two snapshots of the pressure field for the solution with the lowest value for ε are plotted in (c) (at times $t = \frac{1}{3}$ and 20). The plugged region for $t = 20$ is indicated by the red contour in the final snapshot of hS/Bi; the light green lines show some of the characteristics from figure 4, and the white dashed lines show correspondingly chosen contours of constant p_z.

of the slot, generating a rigid plug there. As the interface continues to rise, the plug expands, until at the end of the computation (at $t = 30$), it occupies about half of the bottom of the slot ($z = 0$) and extends almost halfway up the minimum gap towards the free surface. The final state then contains the plug, with a limiting plastic state held at the yield stress arising everywhere else (see the final panel of the figure).

The Charpit analysis of §4 does not account for the appearance of any such plugs. In particular, the plug in the Bi = 2 computation of figure 7 eliminates the characteristics that would otherwise arch upwards from $z = 0$ in the vicinity of the minimum gap. Over the plastically deforming region that is thereby vacated, the characteristic curves must begin at the yield surface instead. This modifies the final state from that considered in §4, and, in particular, appears to allow the numerical solution to evolve towards a state in which no discontinuities arise in the horizontal pressure gradient (see the isobars of the final solution at the bottom right of figure 7). In other words, the plug severs the characteristics from the bath that would normally cross above the red circle in figure 4, and adjusts the overlying characteristics field to prevent any such crossings, as illustrated by the contours of constant $\Xi = p_z$ also plotted for the final snapshot in figure 7. Note that the final solution pictured here has not yet reached steady state, and the plug is still expanding (accounting for slight discrepancies between the contours of constant $\Xi = p_z$ and the characteristic curves from figure 4). Also, despite the apppearance of plug and the implied adjustment of the pressure field, the interface ascends to a final height that is similar to that predicted in §4.

All that said, the numerical solution becomes particularly sensitive to resolution and the regularization parameter in the vicinity of the minimum gap and free surface at late times (see figure 7(b)). This renders the numerical results less reliable, and calls for a numerical algorithm that better accounts for the plugs and any stress discontinuities (such as an augmented Lagrangian scheme [9]). It is conceivable that the late-time solution is plagued by numerical issues, and it cannot be concluded definitively that the final state does not contain any discontinuities in horizontal pressure gradient or crossed characteristics. Nevertheless, the plug appears to be a robust feature of the numerical solution, which must certainly impact the final state.

Finally, figure 8 shows an example with Bi = 1. In this case, the Charpit analysis fails because insufficient information is provided to construct the entire free surface if the fluid reaches the limiting plastic state everywhere.

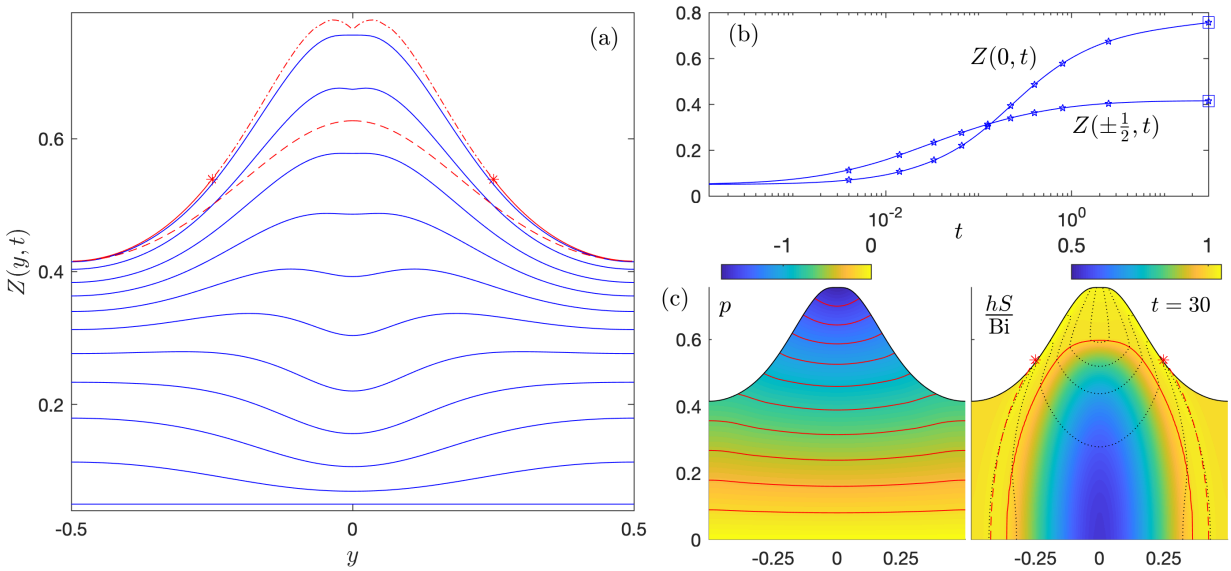

Figure 8: A similar figure to that shown in figures 6 and 7, but for Bi = 1 ($\varepsilon = 10^{-4}$). In (a), the free surface predicted by the Charpit analysis is shown in red, with the same meaning of the star and line style as in figure 4. The red dashed line shows the one-dimensional approximation, $Z = (\mathrm{Bi} + h)$. The plugged region for $t = 30$ is indicated by the red contour in the final snaphsot of hS/Bi in (c); the dashed lines and stars show the final characteristic from the bath to intersect the free surface from figure 4, and the dotted lines are sample contours of constant $\Xi = p_z$.

For the initial-value problem, a plug again forms at the base of the minimum gap as the fluid rises (this time for $t > 1$). Although numerical difficulties again plague the late-time solution, the plug looks to fill most of the slot eventually, leaving a narrower plastic state elsewhere. The emergence of this plug naturally accounts for the failure of the Charpit analysis: only over a small section of the bath are the characteristics launched from $z = 0$, and the yield surface provides the information needed to complete the field of characteristics. Although the fluid is still moving slightly at the end of the computation, the final rise of height largely matches up with the prediction of §4 over the piece of the free surface connected to the bath by uninterrupted characteristics (see figure 8(a)), and the yield surface is approaching the last of those curves. Elsewhere, the interface looks somewhat different to that part constructed inconsistently in the Charpit analysis (shown as the dot-dashed section). It is also worth noting that the interface position for this example is certainly different from the one-dimensional approximation $Z \sim (h + \mathrm{Bi})^{-1}$ (see figures 4 and 8).

6. Conclusions

This paper has considered the capillary rise of a fluid with a yield stress in a Hele-Shaw cell. When the gap is non-uniform, the nonlinear relation between the flux and pressure gradient ensures that sideways variations contribute to dictating the final height of rise. This feature contrasts with the situation for Newtonian fluid, for which each local vertical cross-section can be considered independently in determining the degree of imbibition. Generalizations of Jurin's law that ignore sideways gradients are therefore limited to situations in which the height of rise is much less than the distances over which the gap varies.

A more consistent approach is to use the viscoplastic analogue of the conventional Hele-Shaw approximation, which recasts the problem in the manner of Reynolds lubrication theory for the flow of a yield-stress fluid down a narrow gap. The model that results encapulsates the yield condition as a criterion involving local pressure gradients. The height of capillary rise can then be constructed analytically when the stresses reduce to the yield point throughout the slot. The construction involves finding a set of characteristics for the pressure field in this perfectly plastic limit (similar to viscoplastic spreading problems with a free surface [6, 7], or theory for the flow of highly shear-thinning power-law fluids down slots in models of injection moulding and Saffman-Taylor fingering [10, 11]), and then determining where along these curves the free surface conditions are met.

For a wedge-shaped slot, the construction highlights how lateral gradients become key in controlling the height of rise as the gap closes. Generalizations of Jurin's law that neglect sideways gradients therefore become inaccurate in this limit. However, it turns out that the characteristics construction of the final state is also problematic in the same limit, as one cannot find a complete solution throughout the slot. To understand this difficulty in more detail, we retired to a different problem: the capillary rise of fluid through the annular gap between two offset cylinders. In this alternative problem, it is more straightforward to understand how the characteristics construction fails, and further to instead provide numerical solutions

for the time-dependent rise of the fluid. The numerical solutions demonstrate how the fluid in the lowest and narrowest parts of the slot plug up during the capillary rise, resolving the puzzle of the characteristics.

According to the analysis, the capillary rise expected over the narrowest parts of the lost should significantly exceed that predicted from neglecting sideways gradients. Curiously, this expectation disagrees with the experimental reported by Géraud *et al.* [2]: in their wedge-shaped slots, the rise was not prominent near the corner and no higher than their generalization of Jurin's law. Possible explanations for this discrepancy include the failure of the Hele-Shaw approximation at the corner, or the omission of the full interface curvature and its detailed geometry when computing the capillary pressure and the interfacial motion in the current theory (*cf.* [12]).

References

[1] V. Bertola, Wicking with a yield stress fluid, Journal of Physics: Condensed Matter 21 (3) (2008) 035107.

[2] B. Géraud, L. Jørgensen, L. Petit, H. Delanoë-Ayari, P. Jop, C. Barentin, Capillary rise of yield-stress fluids, EPL (Europhysics Letters) 107 (5) (2014) 58002.

[3] P. Coussot, Saffman–Taylor instability in yield-stress fluids, Journal of Fluid Mechanics 380 (1999) 363–376.

[4] S. H. Bittleston, J. Ferguson, I. A. Frigaard, Mud removal and cement placement during primary cementing of an oil well – laminar non-Newtonian displacements in an eccentric annular Hele-Shaw cell, Journal of Engineering Mathematics 43 (2-4) (2002) 229–253.

[5] D. R. Hewitt, M. Daneshi, N. J. Balmforth, D. M. Martinez, Obstructed and channelized viscoplastic flow in a Hele–Shaw cell, J. Fluid Mech. 790 (2016) 173–204.

[6] N. J. Balmforth, R. V. Craster, R. Sassi, Shallow viscoplastic flow on an inclined plane, J. Fluid Mech. 470 (2002) 1–29.

[7] N. J. Balmforth, R. V. Craster, A. C. Rust, R. Sassi, Viscoplastic flow over an inclined surface, J.Non-Newtonian Fluid Mech. 142 (2007) 219–243.

[8] I. N. Sneddon, Elements of partial differential equations, McGraw-Hill, 1957.

[9] S. Pelipenko, I. Frigaard, Two-dimensional computational simulation of eccentric annular cementing displacements, IMA journal of applied mathematics 69 (6) (2004) 557–583.

[10] G. Richardson, J. King, The Saffman–Taylor problem for an extremely shear-thinning fluid, Quarterly Journal of Mechanics and Applied Mathematics 60 (2) (2007) 161–200.

[11] G. Richardson, J. King, The Hele-Shaw injection problem for an extremely shear-thinning fluid, European Journal of Applied Mathematics 26 (5) (2015) 563–594.

[12] C.-W. Park, G. Homsy, Two-phase displacement in Hele-Shaw cells: theory, Journal of Fluid Mechanics 139 (1984) 291–308.